Chapter 5

MECHANISMS FOR HYDROGEN EVOLUTION FOR CP*RH(BPY)

With contributions from James D. Blakemore, Luis Aguirre-Quintana, Sydney Corona, and William A. Goddard III

Some material adapted from:
L. Aguirre Quintana; **S.I. Johnson**; S.L. Corona; W. Villatoro; W.A. Goddard III; M. K. Takase; D. G. VanderVelde; J. R. Winkler; H. B. Gray; and J.D. Blakemore; Proton-Hydride Tautomerism in Hydrogen Evolution Catalysis. *Proceedings of the National Academy of Sciences* 2016, 113 (23), 6409-6414.

Introduction

In the previous two chapters, solar fuels have presented themselves as a means for solar energy storage.[1,2] However, these chapters focused solely on CO_2 reduction, a scheme in which hydrogen production presents itself as a nuisance. However, in the case where hydrogen is selectively produced, it too is considered a viable solar fuel. In the ideal hydrogen evolution reaction (HER) based solar fuels scheme, a catalyst would use protons and electrons harvested from solar-powered water splitting and convert them to hydrogen.[1,2] This fuel-forming catalyst should be earth-abundant and have a high turnover frequency in order to provide low-cost energy storage. Nonetheless, the atomistic details of even the simplest fuel-forming reaction, combining two H^+ and two e^- with the aid of a catalyst to form H_2, are often poorly understood.

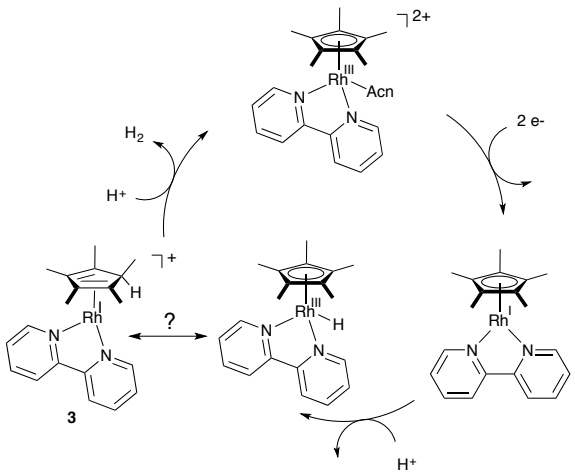

Scheme 5.1: Previous mechanisms for hydrogen evolution in this catalyst involved the generation of a Rh^{III} hydride. Experimentally, protonation of the Cp* is seen.

One example of a hydrogen evolution reaction (HER) catalyst is the Cp*Rh(bpy) catalyst [Cp* = pentamethylcyclopentadienyl, bpy = 2,2'-bipyridine]. This catalyst was originally synthesized by Maitlis et al.[3] and was used in a colloidal suspension by Graetzel et al. to evolve hydrogen.[4] The reduced form of the catalyst was recently isolated and crystallized by Blakemore and coworkers.[5] HER in Cp*Rh(bpy) was previously thought to occur first by a two electron reduction to the Rh^{I} catalyst, followed by protonation at the metal as shown in Scheme 5.1.[4] However, as shown by Aguirre-Quintana et al., upon protonation by a weak acid, triethylammonium ($TEAH^{+}$), protonation of the Cp* ring was observed, with all protonation occurring at the *endo* position (oriented towards the metal center).[6] The presence of the protonated ligand and its position is confirmed via NMR and X-Ray crystallography. With the weaker acid alone, the protonated complex does not produce H_2. However, when the Cp*H complex is in the presence of a stronger acid, protonated dimethylformamide (DMF), HER goes to completion, liberating H_2 with unity yield.[6] Evidence of protonated Cp* ligands in transition metal complexes has been seen[7-9]; this is the first time hydrogen evolution had been seen from a complex of this type. It is also of note that the same intermediate is also seen in water.[10] Understanding the role of this complex is key to better understanding of HER, as several catalysts involving protonated ligands have been successful for HER.[11-13] One catalyst of note, a nickel metalloporphyrin system augmented with a pendant base, has been shown to have two pathways for HER, one operative with weak acids and another operative for the case of strong acids.[11] Neither pathway involves formation of a traditional metal hydride.

In this work we seek to answer how protonation occurs at the Cp* ligand, as well as understand how hydrogen evolution occurs from the singly protonated compound. In this way, we can understand the true nature of Cp*Rh(bpy) as an HER catalyst and potentially use these lessons to develop earth abundant analogues. It is important to study this specific catalyst because of the ubiquity of Cp* as a ligand in organometallic catalysis. The results with this compound contradict the usual notion that Cp* is an inert ancillary ligand. To the contrary, it now seems that Cp*/Cp*H may be a useful interconvertible motif that relies on close ligand-metal cooperation to drive successful catalysis. Towards this goal , density functional theory (DFT) will be used to locate intermediates and transition states along

pathways for evolving hydrogen. In particular, we will be seeking to understand if the protonated ligand is responsible for hydrogen evolution.

Methods

All calculations were performed using density functional theory. Geometry, frequency, and solvation calculations were completed with the B3LYP functional[14,15] modified by a dispersion correction[16] with 6-31G** basis set on organics.[17,18] Rh atoms were treated with the Los Alamos small core potential and 2-ζ basis set.[19] All single point energy calculations were completed with the M06 functional[20], again modified with a dispersion correction.[16] The 6-311G**++ basis was used for on organics. Rh was treated with the 3-ζ LACV3P**++ basis set, augmented with f and diffuse functions.[21,22] Solvation in acetonitrile was applied using the Poisson Boltzmann polarizable continuum model with a dielectric constant and probe radius of 37.5 and 2.19 Å. To calculate the free energy of acetonitrile, the 1 atm ideal gas free energy was calculated and the empirical energy of vaporization, 1.27 kcal/mol was subtracted.[23] Free energies were computed in according to the following equation:

$$G = E_{M06} + G_{solv} + E_{ZPE} + H_{vib} + H_{TR} - T(S_{vib} + S_{elec})$$

Where zero point energies, enthalpic, and entropic effects are provided by frequency calculations at room temperature. To validate calculations with the acids, the pK_a values of triethylammonium ($TEAH^+$) and protonated dimethylformamide (HDMF) were calculated in acetonitrile and compared to experiment. For these calculations, the value of the proton in solution was calculated from its gas phase free energy ($G_{H+} = H - TS = 2.5k_bt - T\times26.04 = -6.3$ kcal/mol) plus the empirical free energy of solvation in water at concentration of 1 M ($\Delta G_{H+,solv} = -265.9 + k_bt \ln(24.5)$), as found by Tissandier et al.[24] To account for solvation in acetonitrile, the free energy of intersolvent proton transfer of 14.1 kcal/mol was used in accordance with measurements by Roberts and coworkers.[25,26] This yields a value of -256.2 kcal/mol for the free energy of the proton solvated in acetonitrile. Using this value, the pk_a of triethylammonium and HDMF in acetonitrile was calculated as 18.5 and 4.0 respectively, which compares well to the experimentally measured value of 18.8 and 6.1. In calculations involving the Rh complexes, the explicit acid complexes themselves were used, rather than the energy of the free proton. All calculations were completed in Jaguar.[27]

Results and Discussion

Routes to First Protonation

First, we aim to show how protonation occurs at the Cp* ring. Scheme 5.2 shows the various protonation routes that can be taken by this catalyst to form the protonated species. In this scheme, all free energies are referenced to **1**, the Rh^{I} species with $TEAH^{+}$ as the acid. Thermodynamically, three intermediate states are available. Complex **2** is downhill by 1.1 kcal/mol and features a traditional Rh^{III} hydride, while complexes **3X** and **3** are the exo and endo Rh^{I} with protonated ligand. These molecules are both exergonic to form in the presence of $TEAH^{+}$ by 7.0 and 7.3 kcal/mol, respectively. The geometry of complex **3** features visible ring slippage in the Cp* moiety, forming an η^4 bound dienyl Cp*H ligand. To form these protonated species, three separate routes are shown.

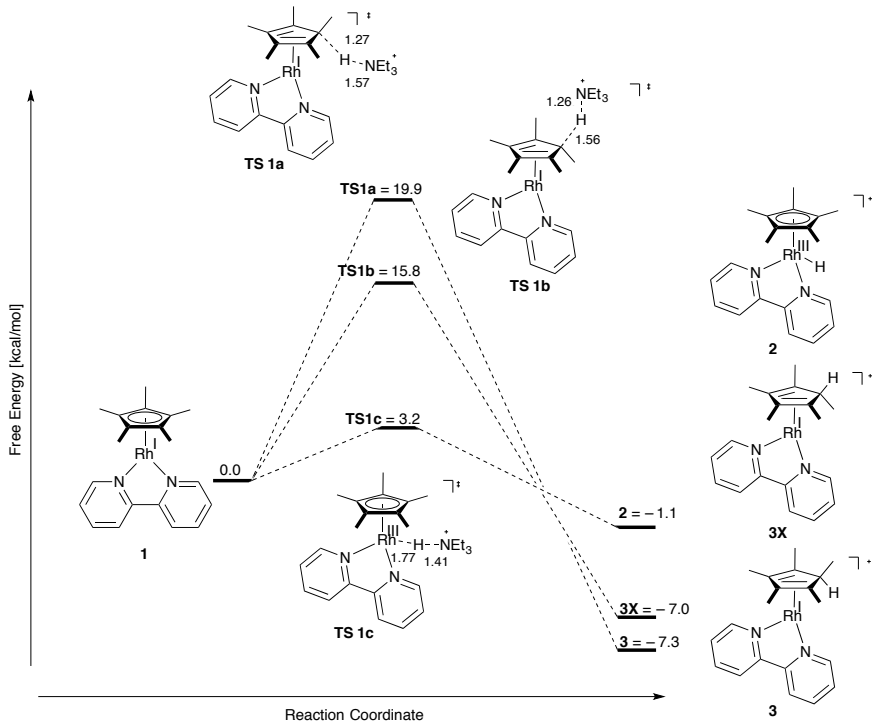

Scheme 5.2: Protonation at the metal center to form the traditional hydride is the most kinetically feasible pathway.

The first is through **TS 1a**, which features direct protonation of the carbon in Cp* by $TEAH^{+}$ to form **3**. In this transition state, the aromaticity of the Cp* ring is broken, allowing the methyl group to bend upwards and the carbon in the ring to accept a proton. The

distance between proton and the carbon on the ring in this transition state is 1.57 Å. At 19.9 kcal/mol, the barrier for this route indicates a kinetically slow reaction, which may be expected due to the similarities between this reaction and C-H activation. This also may be attributed to steric effects, as the $TEAH^+$ is quite bulky. Under this hypothesis, one may surmise that protonation from the top of the Cp* ring may be more favourable. This transition state is demonstrated in **TS 1b**, where the $TEAH^+$ attacks from the top to form the slightly higher in energy *exo* analog, **3X**. This barrier is lower in energy, at a barrier of 15.8 kcal/mol but features a transition state with a slightly shorter H-C_{Cp*} distance of 1.56 Å. The reduced barrier and C-H distance support the fact that steric bulk in the acid plays a role in preventing direct protonation at the ring, but is not the only factor present. The final option is direct protonation of the metal, which is represented by **TS 1c**. At 3.0 kcal/mol, this transition state is the most accessible. At 1.41 Å, this transition state features the longest H-N distance, implying its late nature. This may be a product of sterics, as the $TEAH^+$ is unable to deeply penetrate the cavity left by the metal and the Cp*.

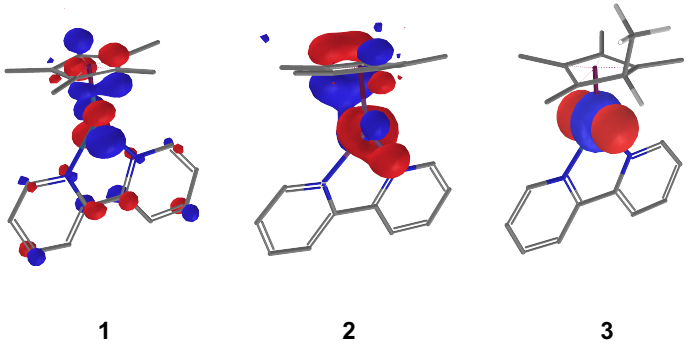

Figure 5.1: Frontier orbitals of complexes **1, 2,** and **3**. While in the original complex the HOMO is delocalized, on **3** it is localized in a dz^2 orbital.

The frontier orbitals of the starting complex, as well as final two thermodynamic products are seen in Figure 5.1. The HOMO in **1** is largely delocalized over the p_z orbitals of the bipyridine, the d_{yz} orbital of the metal, and the p_z orbitals of the carbons in the Cp* ring. Upon protonation at the metal center, the HOMO is made up of a molecular orbital consisting of the s orbital of the hydride, the d_{z2} of Rh, and the π system of the Cp*. In

complex **3**, the HOMO is localized almost solely in in the dz^2 orbital, implying that the Rh behaves formally as a Rh^I center.

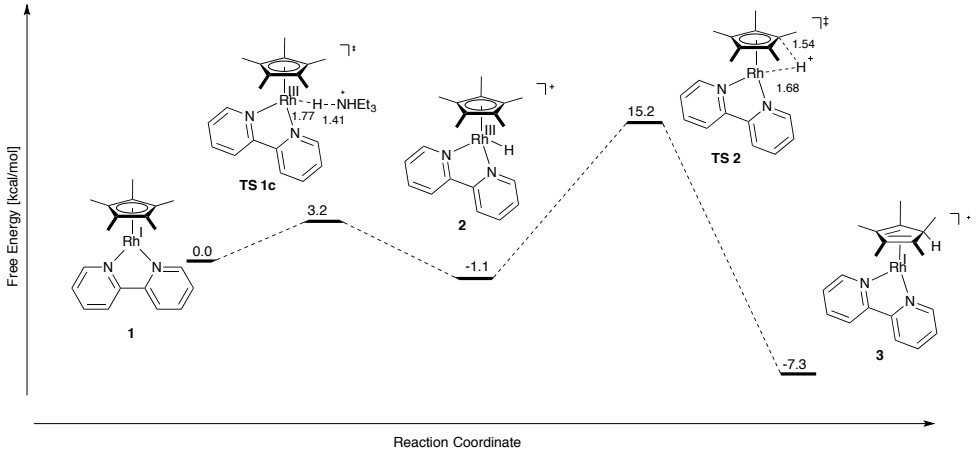

Scheme 5.3: After formation of the hydride, the proton can bridge, forming the Rh^I complex with the protonated Cp* ligand.

While metal protonation is the most kinetically feasible, it is still true that the thermodynamically preferred and experimentally observed complex is **3**. The product **2** features a long Rh-H bond of 1.56 Å, which implies that it is rather weak; however, it is a true hydride and is not bridging to the Cp* (as evidenced by the distance: $H\text{-}C_{Cp^*}$ = 2.72 Å). Due to the weak Rh-H bond, a transition state between **2** and **3** may be feasible. This is shown in Scheme 5.3. From **2**, the proton is able to bridge to the Cp* with a thermally accessible barrier of 15.2 kcal/mol. The reverse reaction from the protonated Cp* complex to the Rh^{III} is 22.5 kcal/mol higher, which is likely insurmountable at room temperature. In the weak acid case, this is the product and no hydrogen is produced.

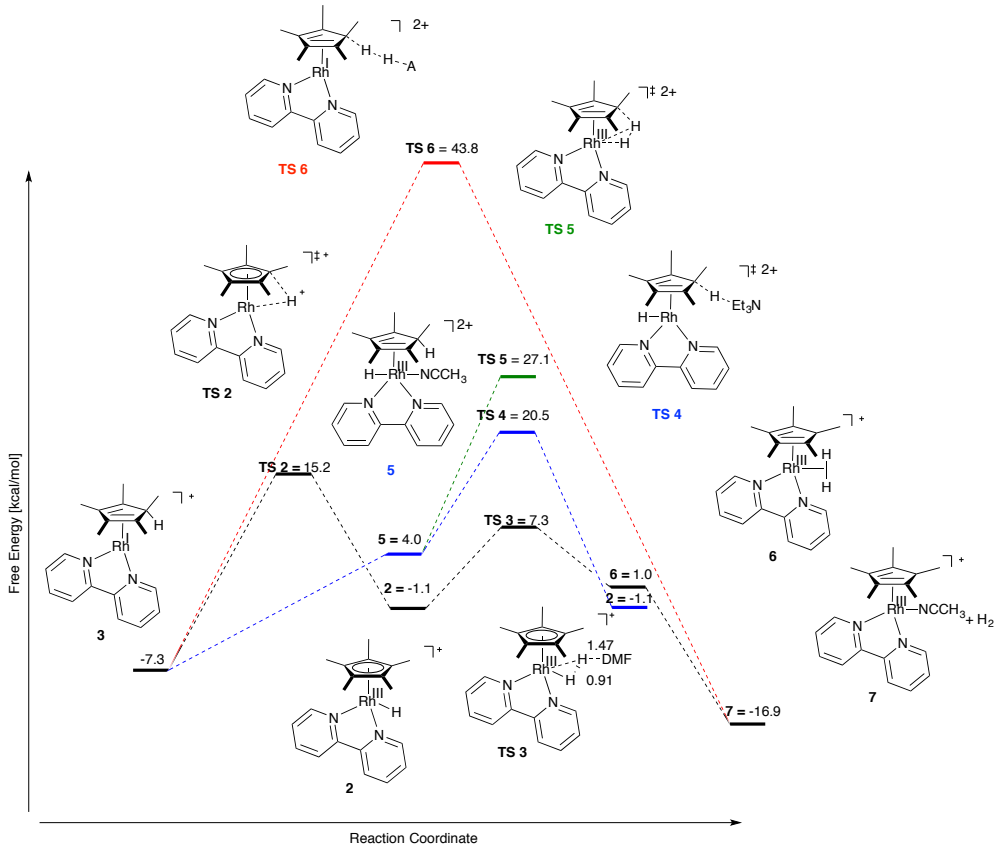

Scheme 5.4: Routes involving a second protonation by HDMF. Energies in kcal/mol and bond lengths in Ångstroms.

*Protonation from the Cp*H complex*

In the presence of a stronger acid HDMF (protonated dimethylformamide, pK_a = 6.1), hydrogen is evolved, both from the starting complex **1** and the resulting complex **3**. Various routes for this process is shown in Scheme 5.4. From the starting state **3**, several mechanisms for the formation of hydrogen can be seen. Direct acid attack at the protonated Cp*H can be seen in **TS 6**, wherein Cp*H acts as an organic hydride donor. As had been previously shown, the HOMO in **3** is largely localized on the Rh center as a formal Rh^{I}. This means that the electron density to make the hydride must be passed through the π system of the Cp* ring in order to form the hydride. The calculated barrier for this reaction is 43.8 kcal/mol, far too high for a room temperature H_2 evolution reaction. This high barrier is somewhat to be expected, as second order rate constants for hydride transfer from aryl rings

to carbocation hydride acceptors are often several orders of magnitude smaller than their transition metal hydride cousins.[28-30]

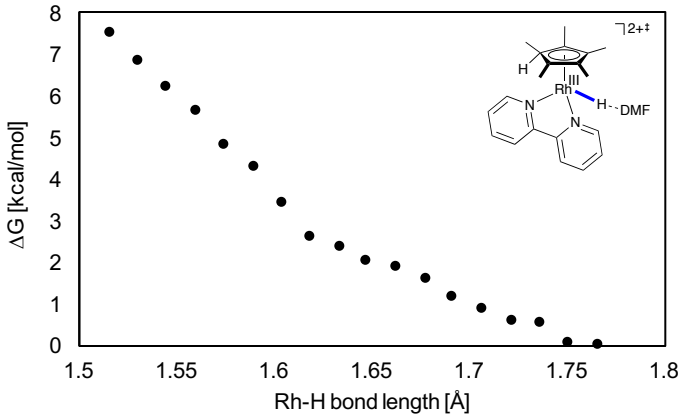

Figure 5.2: Relaxed coordinate scan moving the Rh-H distance 0.015 Å each step.

Alternatively, the protonated Cp* complex **3** can undergo a barrierless second protonation, as shown in blue to form **5**. Complex **5** is the *trans* isomer of the doubly protonated complex and the lowest energy isomer of all possible combinations. It features a loosely coordinated acetonitrile opposite the hydride. The analogue sans acetonitrile is higher in energy by 8 kcal/mol. The *cis* isomers with and without acetonitrile are higher in energy by 3.3 and 15.1 kcal/mol, respectively. In order to establish the barrierless nature of the protonation to form **5**, a relaxed coordinate scan of the Rh-H bond distance from 1.766 to the resting distance of 1.516 Å with a step size of 0.015 Å was completed. The results of the scan can be seen in Figure 5.2, in which he energy is monotonically increasing with decreasing Rh-H distance. From **5**, the potential energy surface branches into two potential routes. The higher barrier route through **TS 5** involves a metathesis pathway, wherein the Cp* ring rotates and the proton from the ring is passed back to the metal. The geometry of this transition state is unique, as the proton is not passed directly from overhead to the metal-bound proton, but rather from a slightly rotated position onto the Rh (dihedral angle ∠ H-Rh-C-H of 45.0°). A representation of this geometry is shown in Figure 5.3a. In theory, this would go on to form **6**, the dihydrogen complex present as a short lived intermediate before the thermodynamically favored release of hydrogen, shown by **7**. However, at a barrier of 27.1 kcal/mol, this is also unfeasible at room temperature for hydrogen evolution.

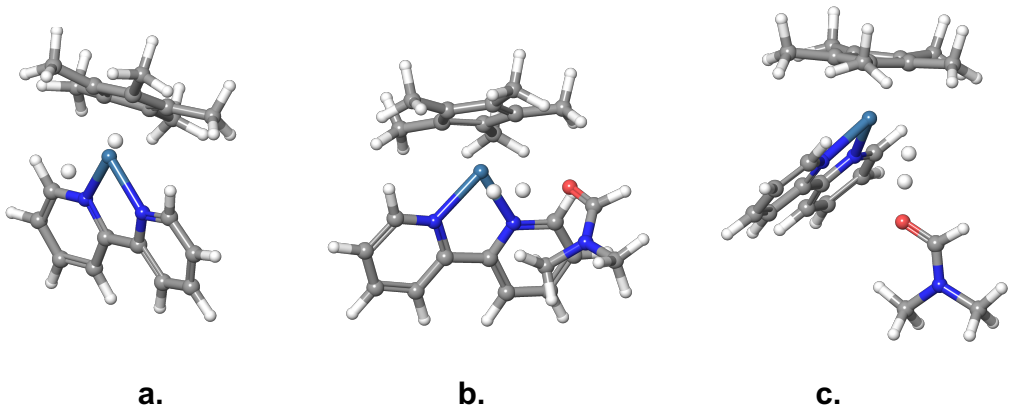

Figure 5.3: Relevant transition states, a. **TS 5**; b. **TS 3**; c. Attack on hydride from bottom.

It is important to note that in the experimental system, two equivalents of HDMF are added. The first equivalent protonates the TEA in solution, which completed the first protonation. The second equivalent is then thought to provide the second proton for the formation of H_2, supported by gas chromatograpy measurements.[6] Especially while the first equivalent of HDMF is being added, some TEA may be available in solution to abstract a proton. In some heterogeneous systems, protonation occurs at one location to stabilize the system for a second protonation, only to be abstracted later.[31] This is shown by the alternative transition state **TS 4**, wherein TEA abstracts a proton from the ring to form the singly protonatated hydride **2**. The barrier for this is similarly high at 20.5 kcal/mol. The analogous transition state with DMF acting as base has a higher barrier of 24.5 kcal/mol, which is reasonable considering that TEA is more basic than DMF. These transition states rule out participation by the protonated Cp*, leaving only those routes involving the traditional hydride and concerted routes and.

Two routes exist from the traditional hydride **2**. The first, **TS 3**, features a side-on attack from HDMF to form the dihydrogen adduct **6**. This barrier is quite feasible at 7.3 kcal/mol, which is only 8.4 kcal/mol uphill from **3**. The geometry of this complex can be seen in Figure 5.3b. In this transition state, the Rh-H length of 1.71 Å is lengthened from the previous Rh-H bond length of 1.56 Å, but is not as far as the dihydride adduct (**6**) Rh-H lengths of 1.93 Å. The H-H bond length in the transition state is 0.91 Å and relaxes to a bond length in **6** to 0.783 Å. This H-H bond length is indicative of a classical hydrogen

complex, rather than a bound H_2, or a dihydride.[32] This implies that in this transition state, we are moving from a hydride to a very loosely bound H_2 adduct that may be short lived, if exists at all.

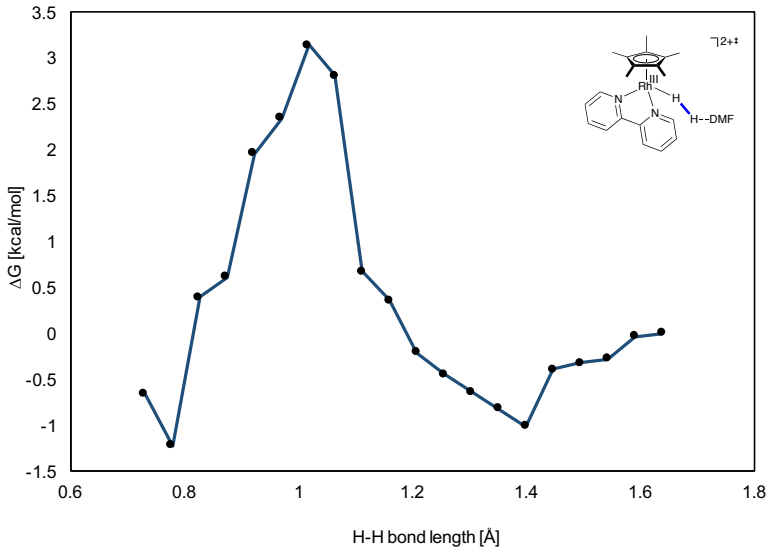

Figure 5.4: Potential energy surface along a decreasing H-H bond distance with acid attack from the bottom.

A second route found via a relaxed coordinate scan features attack from the bottom in the direction of the bipyridine ligand. The full free energy surface for this is shown in Figure 5.4. The coordinate scan began with a minimized Rh-H species **3** with HDMF nearby, which is taken as the reference state for this calculation. The H-H bond distance was then shortened by 0.048 Å and the new geometry was minimized at each step. The process repeated itself for H-H distances ranging from 1.638 to 0.538 Å, though only distances to 0.729 Å are included in this plot. Distances smaller than this showed a large increase in energy due to atomic repulsion. At each point, the full free energy including enthalpies and entropies is calculated. As the H-H interatomic distance is decreased, a shallow well centered around H-H = 1.399 Å develops, though the energy of this well (~1 kcal/mol) is smaller than the accepted error for DFT. This is followed by a barrier in the potential energy surface of 3.1 kcal/mol at an H-H distance of 1.016 Å. This is an earlier transition state that the side-on attack, as both the H-H and the protic H-O distance are much closer to the corresponding distances in the reactants. Similarly, the Rh hydride distance of 1.66 Å implies

the early nature of the transition state. A representation of the complex at the maximum along the potential energy surface is seen in Figure 5.3c. As the H-H distance continues to decrease, the barrier is overcome and a minimum of -1.2 kcal/mol is seen at an H-H distance of 0.777 Å. In this state, the Rh-H distances are 1.86 and 2.08 for the original hydride and proton respectively. This geometry could imply that **6** never truly forms in solution. However, it is of note that both low barrier hydride protonation routes involve participation of both the hydride and the metal, a scheme seen previously in biological[33,34], heterogeneous[31], and inorganic[35,36] systems. It is also important to note that both low barrier pathways occurring via the hydride lower in energy than protonation via the bridging pathway, **TS 2**. In the presence of strong acid, it is likely that the ring will not participate as fast kinetics will drive the system towards hydrogen evolution. While this suggests that **3** is off-path in the strong acid case, it is on path in the weak acid case. Previous work by Solis et al. has identified other HER catalysts where two separate cycles exist for differing acid strengths.[11] Both works imply that in kinetic studies, it is important to consider that multiple paths can exist that are accessible in differing conditions.

In isolation, formation of the hydride species **2** from **3** encounters a barrier of 22.5 kcal/mol, which is quite high. However, a concerted route by which the protons approach simultaneously is a possibility. As an isolated transition state, this proved quite difficult to locate. However, the same step approach used in Figures 5.2 and 5.3 was used here, except with two variables rather than one. The first variable was the Rh-H distance, where the proton in question is the one bound to Cp*. This distance was increased in increments of 0.260 Å. The second variable was the distance between the proton on the Cp* and the proton of the acid, which was decreased in increments of 0.250 Å. This resulted in 42 individual geometries and energies, which can be seen in the contour plot in Figure 5.5.

One can see several critical points, the geometries of which are included in the figure. Point A is a local minimum which represents the protonated Cp* complex, **2**, with the acid nearby. Another critical point can be seen in B., where the proton has migrated to form a loosely bound hydride (Rh-H distance of 1.697 Å), with the acid oriented towards it. This state is interesting, as it shows a shallow minimum in preparation for protonation of the hydride. The final critical point, C, is the point post-protonation, where H_2 has been released and can

go into solution. One additional feature is the barrier in the top middle of the figure. This large barrier is one previously discussed, **TS 6**, where HER occurs directly from the **2**.

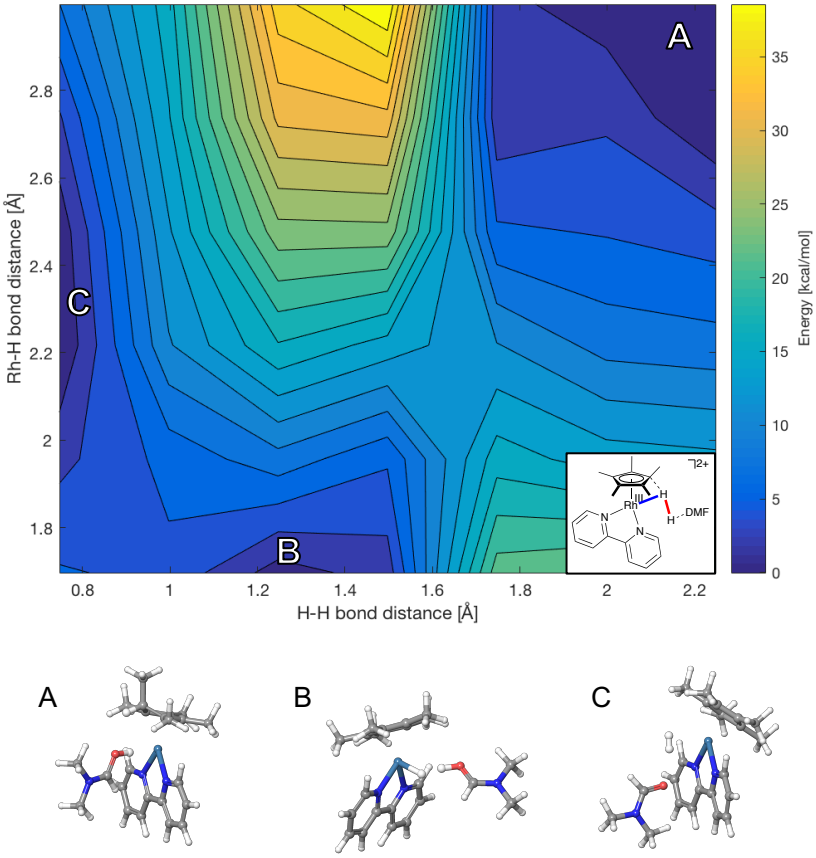

Figure 5.5: Varying the H-H distance and the Rh-H distances yields several critical points of interest, geometries of which can be seen in A., B., and C.

The path connecting A and B features a barrier around ~12 kcal/mol, which is lower than the defined barrier in **TS 2** and is, more importantly, accessible at room temperature. The barrier is reduced by the simultaneous movement of the proton on Cp* towards Rh and the two protons together. The figure suggests that the potential energy surface for this system is quite flat. The barrier region itself is quite broad, which indicates why a transition state was difficult to locate. A higher resolution search (which is in the works) will yield more information. However, this implies that from **2**, a concerted route towards B and then towards C, with the release of H_2, is the only feasible path towards hydrogen production.

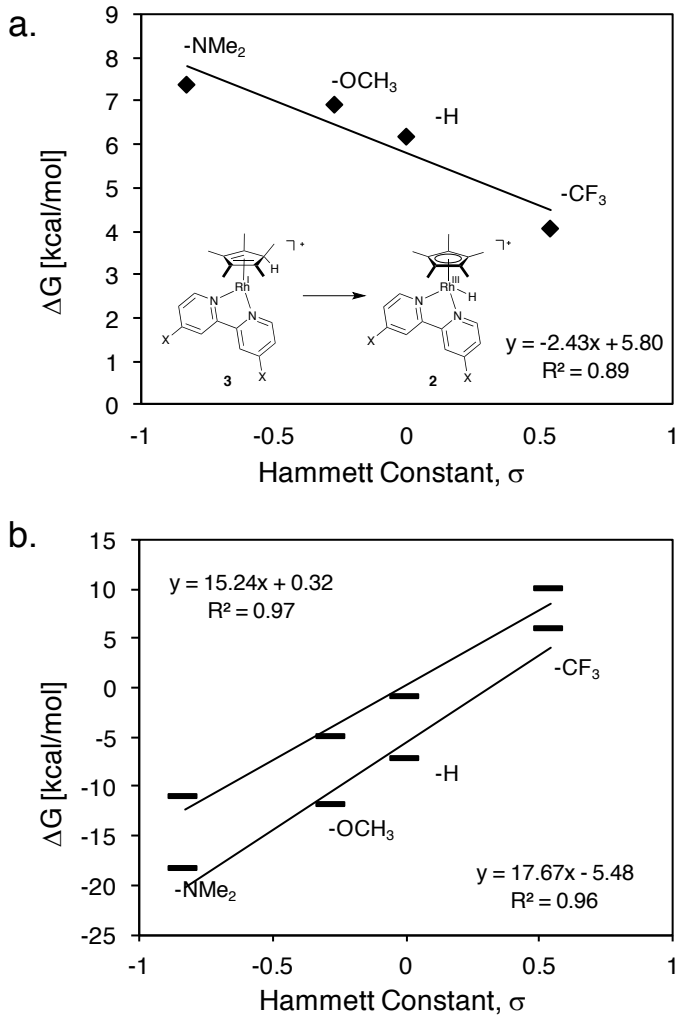

Figure 5.6: 5.6a.) Linear correlation between the Hammett constant of functional groups on bpy and energy difference between complexes 2 and 3 shows the effect of bpy on this complex. 5.6b.) As the functional groups become more electron withdrawing, the complex becomes harder to protonate.

In order to gauge substituent effects on the electronic structure of the Cp*Rh(bpy) complex, several functional groups were substituted in the *para* position of the bipyridine ligand. The computationally calculated difference between the protonated Cp* ligand and the Rh^{III} hydride was plotted against the Hammett constant (σ_p) of the functional groups in Figure 5.6a. Hammett constants ranging from -0.83 to 0.54 (electron donating to withdrawing) were used.[37] There is a linear relationship between ΔG and σ_p, suggesting that within the bpy

family, variation of the electronic structure is quite small. Though not shown here, this is also corroborated by little change in the Mulliken populations of the nitrogen, rhodium, and relevant carbon atoms among different functional groups. One implication that can be gleaned from this is that in order to favor the formation of the hydride, 2, a functional group with a Hammett constant of ~2.5 would be needed, suggesting that only an incredibly electron donating group can achieve this within the bpy family. It would thus seem that the bpy backbone is very adept at absorbing the electronic effect of the functional group, making it an excellent candidate for surface attachment. One could surmise that a bpy-based rhodium catalyst bound to a surface would likely perform similarly to the homogeneous analog.

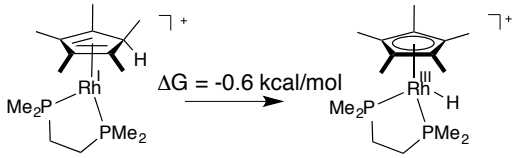

3DMPE **2DMPE**

Scheme 5.5: The hydride is slightly favored in phosphine-based ligand sets.

Intuitively, one might expect the more electron donating ligands to have a smaller ΔG between complexes **2** and **3**, as more electron density on the metal would favor the formation of the hydride. Nonetheless, this is not seen. Reasons for this can be seen in Figure 5.6b, in which the energy to protonate **2** and **3** from **1** are plotted against Hammett Constant. As the bpy ligand becomes more electron withdrawing, the overall metal complex becomes harder to protonate. This effect is felt more strongly at the metal center and the hydride becomes harder to form more rapidly with respect to electronic effects than the protonated Cp*, as indicated by the differing slopes of the trend lines.

However, once one travels outside the bpy family, one sees a different story. Using 1,2-bis(dimethylphosphino)ethyl (dmpe) groups instead of bpy in a toy system, the ΔG is shifted just slightly in favor of the Rh^{III} hydride, as shown in Scheme 5.5. Previously a diphosphine Rh hydride had been seen with the loss of a Cp*H complex upon exposure to H_2.[8] Examination of the Mulliken populations shows significantly less positive character on the

rhodium atom, showing the electron-donating role of the phosphine groups. This implies that binding to the Cp* is not a given, but rather a characteristic of the molecule as a whole. The bpy ligand depletes the Rh metal center of electron density, resulting in a weak metal hydride bond. This weak bond is so disfavored thermodynamically that it is exchanged for the stronger C-H bond at the cost of some aromaticity in the Cp* ring.

Conclusions

In this study, we have investigated the formation of the unique Cp*H adduct in Cp*Rh(bpy), showing that protonation by a weak acid first occurs at the metal and then the proton bridges to the Cp* to form the *endo* protonated thermodynamic product. This complex is competent for hydrogen evolution upon exposure to HDMF and does so through a combined bridge/protonation pathway. Under exposure to a strong acid, the ring is never likely implicated. Modification of the bpy ligand shows that the thermodynamic product is always the protonated Cp* ligand. However, this changes with the use of diphosphine ligands. This study and catalyst highlight the many accessible pathways to HER, which may be achieved by simply differing conditions in a single catalyst. In some respects, it serves as a cautionary tale for kinetic studies, as the "slower" path may not be the dominant one in typical catalysis.

References

(1) Gray, H. B. *Nat. Chem.* **2009**, *1*, 7-7.
(2) Lewis, N. S.; Nocera, D. G. *Proc. Natl. Acad. Sci. USA* **2006**, *103*, 15729-15735.
(3) Maitlis, P. M. *Acc. Chem. Res.* **1978**, *11*, 301-307.
(4) Kölle, U.; Grützel, M. *Angew. Chem. Int. Ed.* **1987**, *26*, 567-570.
(5) Blakemore, J. D.; Hernandez, E. S.; Sattler, W.; Hunter, B. M.; Henling, L. M.; Brunschwig, B. S.; Gray, H. B. *Polyhedron* **2014**, *84*, 14-18.
(6) Quintana, L. M. A.; Johnson, S. I.; Corona, S. L.; Villatoro, W.; Goddard, W. A.; Takase, M. K.; VanderVelde, D. G.; Winkler, J. R.; Gray, H. B.; Blakemore, J. D. *Proc. Natl. Acad. Sci. USA* **2016**, *113*, 6409-6414.
(7) Gusev, O. V.; Denisovich, L. I.; Peterleitner, M. G.; Rubezhov, A. Z.; Ustynyuk, N. A.; Maitlis, P. M. *J. Organomet. Chem.* **1993**, *452*, 219-222.
(8) Jones, W. D.; Kuykendall, V. L.; Selmeczy, A. D. *Organometallics* **1991**, *10*, 1577-1586.
(9) Zamorano, A.; Rendón, N.; Valpuesta, J. E. V.; Álvarez, E.; Carmona, E. *Inorg. Chem.* **2015**, *54*, 6573-6581.
(10) Pitman, C. L.; Finster, O. N. L.; Miller, A. J. M. *Chem. Comm.* **2016**, *52*, 9105-9108.
(11) Solis, B. H.; Maher, A. G.; Dogutan, D. K.; Nocera, D. G.; Hammes-Schiffer, S. *Proc. Natl. Acad. Sci. USA* **2016**, *113*, 485-492.
(12) Solis, B. H.; Maher, A. G.; Honda, T.; Powers, D. C.; Nocera, D. G.; Hammes-Schiffer, S. *ACS Catal.* **2014**, *4*, 4516-4526.
(13) Lacy, D. C.; Roberts, G. M.; Peters, J. C. *J. Am. Chem. Soc.* **2015**, *137*, 4860-4864.
(14) Becke, A. D. *J. Chem. Phys.* **1993**, *98*, 5648-5652.
(15) Lee, C. T.; Yang, W. T.; Parr, R. G. *Phys. Rev. B* **1988**, *37*, 785-789.
(16) Grimme, S.; Antony, J.; Ehrlich, S.; Krieg, H. *J. Chem. Phys.* **2010**, *132*, 154104.
(17) Francl, M. M.; Pietro, W. J.; Hehre, W. J.; Binkley, J. S.; Gordon, M. S.; Defrees, D. J.; Pople, J. A. *J. Chem. Phys.* **1982**, *77*, 3654-3665.
(18) Hehre, W. J.; Ditchfie.R; Pople, J. A. *J. Chem. Phys.* **1972**, *56*, 2257-2261.
(19) Hay, P. J.; Wadt, W. R. *J. Chem. Phys.* **1985**, *82*, 299-310.
(20) Zhao, Y.; Truhlar, D. G. *Theor. Chem. Acc.* **2008**, *120*, 215-241.
(21) Krishnan, R.; Binkley, J. S.; Seeger, R.; Pople, J. A. *J. Chem. Phys.* **1980**, *72*, 650-654.
(22) Clark, T.; Chandrasekhar, J.; Spitznagel, G. W.; Schleyer, P. V. *J. Comp. Chem.* **1983**, *4*, 294-301.
(23) Bridgeman, O. C., Aldrich, E.W., *J. Heat Transfer* **1964**, *86*, 279-286.
(24) Tissandier, M. D.; Cowen, K. A.; Feng, W. Y.; Gundlach, E.; Cohen, M. H.; Earhart, A. D.; Coe, J. V.; Tuttle, T. R. *J. Phys. Chem. A* **1998**, *102*, 7787-7794.
(25) Pegis, M. L.; Roberts, J. A. S.; Wasylenko, D. J.; Mader, E. A.; Appel, A. M.; Mayer, J. M. *Inorg. Chem.* **2015**, *54*, 11883-11888.
(26) Roberts, J. A. S.; Bullock, R. M. *Inorg. Chem.* **2013**, *52*, 3823-3835.
(27) Bochevarov, A. D.; Harder, E.; Hughes, T. F.; Greenwood, J. R.; Braden, D. A.; Philipp, D. M.; Rinaldo, D.; Halls, M. D.; Zhang, J.; Friesner, R. A. *Int. J. Quantum Chem.* **2013**, *113*, 2110-2142.
(28) Horn, M.; Schappele, L. H.; Lang-Wittkowski, G.; Mayr, H.; Ofial, A. R. *Chem. Eur. J.* **2013**, *19*, 249-263.
(29) Cheng, T.-Y.; Brunschwig, B. S.; Bullock, R. M. *J. Am. Chem. Soc.* **1998**, *120*, 13121-13137.
(30) Mayr, H.; Lang, G.; Ofial, A. R. *J. Am. Chem. Soc.* **2002**, *124*, 4076-4083.
(31) Huang, Y.; Nielsen, R. J.; Goddard, W. A.; Soriaga, M. P. *J. Am. Chem. Soc.* **2015**, *137*, 6692-6698.
(32) Crabtree, R. H. *Chem. Rev.* **2016**, *116*, 8750-8769.
(33) Eilers, G.; Schwartz, L.; Stein, M.; Zampella, G.; de Gioia, L.; Ott, S.; Lomoth, R. *Chem. Eur. J.* **2007**, *13*, 7075-7084.
(34) Carroll, M. E.; Barton, B. E.; Rauchfuss, T. B.; Carroll, P. J. *J. Am. Chem. Soc.* **2012**, *134*, 18843-18852.
(35) Besora, M.; Lledos, A.; Maseras, F. *Chem. Soc. Rev.* **2009**, *38*, 957-966.
(36) O'Reilly, M. E.; Johnson, S. I.; Nielsen, R. J.; Goddard, W. A.; Gunnoe, T. B. *Organometallics* **2016**.
(37) Hansch, C.; Leo, A.; Taft, R. W. *Chem. Rev.* **1991**, *91*, 165-195.